ELSEVIER

International Journal of Fatigue 22 (2000) 495–511

International Journal of Fatigue

www.elsevier.com/locate/ijfatigue

Strain-controlled fatigue properties of steels and some simple approximations

M.L. Roessle [1], A. Fatemi [*]

Department of Mechanical, Industrial, and Manufacturing Engineering, The University of Toledo, Toledo, Ohio 43606, USA

Received 20 February 1999; received in revised form 5 August 1999; accepted 4 February 2000

Abstract

In this study, first strain-controlled deformation and fatigue data are reported and compared for several steels most commonly used in the ground vehicle industry. Correlations between monotonic tensile data and constant amplitude strain-controlled fatigue properties are then investigated, and validity of some of the more commonly used methods of estimating fatigue properties is examined. A simple method requiring only hardness and modulus of elasticity is proposed for estimation of the strain–life curve. Prediction capability of this method is evaluated for steels with hardness between 150 and 700 *HB* and compared with several other methods proposed in the literature. The proposed method is shown to provide good approximations of the strain–life curve.

Keywords: Strain-controlled fatigue; Fatigue property correlations; Strain-life approximations; Cyclic deformation; Low-cycle fatigue; Fatigue life prediction

1. Introduction

Mechanical properties determined from monotonic tensile tests are often used in the design of components. However, in service, most components experience cyclic loading and the fatigue properties of the materials are, therefore, of utmost importance to design engineers. Over the years, many researchers have attempted to develop correlations among the monotonic tensile data and fatigue properties of materials. Such correlations are desirable, considering the amount of time and effort required to obtain the fatigue properties, as compared to the monotonic tensile properties. If reliable correlations with reasonable accuracy can be established, durability performance predictions and/or optimization analyses can be performed, while substantially reducing time and cost associated with material fatigue testing.

The traditional approach to predict crack initiation or nucleation life is based on nominal stress, referred to as the *S–N* approach. The relationship (often referred to as Basquin's equation) can be represented as:

$$\Delta S/2=\sigma_f'(2N_f)^b \tag{1}$$

where $\Delta S/2$ is the stress amplitude and $2N_f$ is the number of reversals to failure. The two fatigue properties needed in this equation are the fatigue strength coefficient, σ_f', and the fatigue strength exponent, b. A second common and more recent approach is based on local strain, referred to as the strain–life (ε–N) method. This approach relates the reversals to failure, $2N_f$, to the strain amplitude, $\Delta\varepsilon/2$. The relationship (often referred to as the Coffin–Manson relationship) is as follows:

$$\frac{\Delta\varepsilon}{2}=\frac{\Delta\varepsilon_e}{2}+\frac{\Delta\varepsilon_p}{2}=\frac{\sigma_f'}{E}(2N_f)^b+\varepsilon_f'(2N_f)^c \tag{2}$$

where $\Delta\varepsilon/2$, $\Delta\varepsilon_e/2$, and $\Delta\varepsilon_p/2$ are the total, elastic, and plastic strain amplitudes, respectively. In this equation, the two additional fatigue properties needed are the fatigue ductility coefficient, ε_f', and the fatigue ductility exponent, c. The strain-based approach considers the plastic deformation that often occurs in localized regions where cracks nucleate. Also, the strain-based approach may be regarded as a comprehensive approach describing both elastic and inelastic cyclic behavior of a

* Corresponding author. Tel.: +1-419-530-8213; fax: +1-419-530-8206.

E-mail address: afatemi@eng.utoledo.edu (A. Fatemi).

[1] Formerly Research Assistant, Currently at Tenneco Automotive.

0142-1123/00/$ - see front matter
PII: S0142-1123(00)00026-8

material. This approach is now commonly used in fatigue design, particularly in the ground vehicle industry.

This study was undertaken by the American Iron and Steel Institute (AISI) to obtain and compare strain-controlled deformation and fatigue properties for 20 steels commonly used in the ground vehicle industry. These data have not been published previously. The data from these steels in addition to 49 other steels published by the American Society of Metals (ASM) in [1] were then used to examine correlations among the various monotonic and fatigue properties. These include relationships among ultimate tensile strength, fatigue limit, fatigue strength coefficient, and hardness, as well as estimation of strain–life fatigue properties and approximation of strain–life curves.

2. Experimental program

2.1. Materials

The materials used in the experimental investigation consisted of SAE 1141, SAE 1038, SAE 1541, SAE 1050, and SAE 1090 steels. The SAE 1141 steels are resulfurized steels with medium carbon content and have grain refinement additives. The SAE 1038, SAE 1050, and SAE 1541 steels are plain carbon steels with medium carbon content. For SAE 1038 and SAE 1050, the maximum allowable amount for Mn is 1.00%, whereas for SAE 1541 the maximum range for Mn is between 1.00% and 1.65%. The SAE 1090 steels are plain carbon steels with high carbon content. The overall range of ultimate tensile strength, S_u, was 582 MPa to 2360 MPa and the overall range of Brinell hardness, *HB*, was 163 to 536. Table 1 provides a summary of the materials used, including material identification, processing condition, grain structure and size, and hardness. The average grain size is represented by an ASTM grain size number and is inversely proportional to the average grain diameter. Anisotropy was minimal, if any, for all materials, as judged by similarities in the transverse and longitudinal average grain sizes and respective hardness values.

2.2. Specimen

Identical round specimens were used for all tests. The specimen configuration and dimensions are shown in Fig. 1. The secondary radius in the gage section causes the minimum diameter to occur in the middle of the test section and compensates for the slight stress concentration that occurs at the shoulders. The stress concentration factor due to this secondary radius in the gage section is very small, K_t=1.017. The specimens were machined from the longitudinal direction (i.e. rolling direction) of the raw material. A commercial round-specimen polishing machine was used to polish the specimen gage section with polishing marks coinciding with the specimen's longitudinal direction. The polishing procedure produced a mirror-like surface finish within the test section for all the materials tested.

2.3. Test equipment and procedures

Servo-controlled hydraulic axial load frames in conjunction with digital controllers were used to conduct the tests. Hydraulically operated grips using universal tapered collets were employed to secure the specimen ends in series with the load cell. Epoxy was used to protect the specimen surface from the knife-edges of the extensometer. Significant effort was put forth to align the load train (load cell, grips, specimen, and actuator). Misalignment can result from both tilt and offset between the central lines of the load train components. ASTM Standard E1012 [2] was followed to verify specimen alignment. All tests were conducted at room temperature.

The monotonic tension tests were performed using test methods specified by the ASTM Standard E8 [3]. After the tension tests were concluded, the broken specimens were reassembled and the final gage length, the final diameter, and the neck radius were measured.

All constant amplitude fatigue tests were performed according to the ASTM Standard E606 [4]. For each material tested, 18 specimens at 6 different strain amplitudes ranging between 0.15% to 1.5% (with 3 duplicate tests for each strain amplitude) were utilized. All tests were conducted under completely reversed strain conditions, $R=\varepsilon_{min}/\varepsilon_{max}=-1$. Failure of the specimens was defined as the point at which the maximum load decreased by approximately 50% because of a crack or cracks being present, as recommended by the ASTM Standard E606 [4]. Strain control was used in all tests, except for long life and run-out tests due to limitations of the extensometer at high frequencies. For these tests (greater than 10^5 cycles), strain control was used initially to determine the stabilized load. Then load control was used for the remainder of the test. For the strain-controlled tests the applied frequencies ranged between 0.1 Hz to 3.5 Hz, with approximately a constant strain rate. For the load-controlled tests the frequency was increased up to 35 Hz or higher in order to shorten the overall test duration. All tests were conducted using a triangular waveform.

3. Experimental results

3.1. Monotonic and cyclic deformation behaviors and properties

The properties determined from the monotonic tensile tests were modulus of elasticity, *E*, yield strength at

Table 1
Summary of materials

Material[a]	Material ID	Processing condition	Grain type	ASTM grain size	Brinell hardness
SAE 1141 (AlFG)	A1	Normalized at 1650 °F	ferrite/pearlite	10 to 11	223
SAE 1141 (AlFG)	A2	Reheat, Q and T	martensite	NA	277
SAE 1141 (NbFG)	A3	Normalized at 1650 °F	ferrite/pearlite	7 to 9	199
SAE 1141 (NbFG)	A4	Reheat, Q and T	martensite	NA	241
SAE 1141 (VFG)	A5	Normalized at 1650 °F	ferrite/pearlite	6 to 8	217
SAE 1141 (VFG)	A6	Reheat, Q and T	martensite	NA	252
SAE 1141 (VFG)	A7	Normalized at 1750 °F	ferrite/pearlite	6 to 8	229
SAE 1038	B1	Normalized at 1650 °F	ferrite/pearlite	8 to 9	163
SAE 1038	B2	Cold size/form	ferrite/pearlite	8 to 10	185
SAE 1038	B3	Reheat, Q and T	ferrite/spher. pearlite	10 to 11	195
SAE 1541	C1	Normalized at 1650 °F	ferrite/pearlite	10	180
SAE 1541	C2	Cold size/form	ferrite/pearlite	10	195
SAE 1050(M)	D1	Normalized at 1650 °F	ferrite/pearlite	9 to 9½	205
SAE 1050(M)	D2	Hot forge, cold extrude	ferrite	7.2 (ferrite)	220
SAE 1050(M)	D3	Induction through-hardened	martensite	NA	536
SAE 1090	E1	Normalized at 1650 °F	pearlite	NA	259
SAE 1090(M)	E2	Hot form, accelerated cool	pearlite/martensite	NA	357
SAE 1090	E3	Hot form, Q and T	martensite	NA	309
SAE 1090	E4	Hot form, austemper	martensite/bainite	NA	279
SAE 1090(M)	E5	Hot form, accelerated cool	pearlite/martensite	NA	272

[a] AlFG: aluminum fine grain; NbFG: niobium fine grain; VFG: vanadium fine grain; M: modified chemical composition.

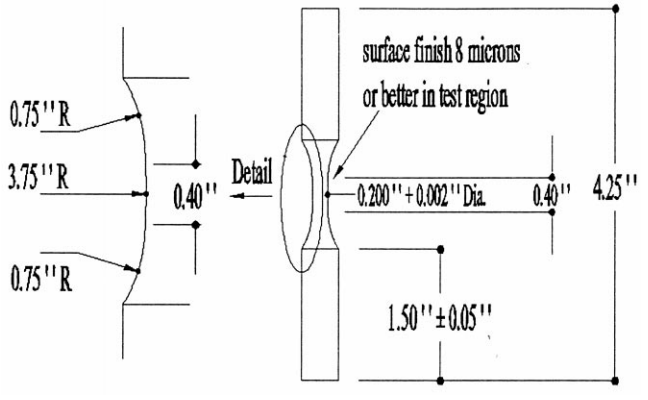

Fig. 1. Specimen configuration and dimensions (courtesy of Dr T. Topper).

0.2% offset, *YS*, ultimate tensile strength, S_u, percent elongation, %*EL*, percent reduction in area, %*RA*, true fracture strength, σ_f, true fracture ductility, ε_f, strength coefficient, *K*, and strain hardening exponent, *n*. The true fracture strength was corrected for necking according to the Bridgman correction factor [5]. The true fracture ductility was calculated from the relationship based on constant volume assumption:

$$\varepsilon_f = \ln\left(\frac{A_0}{A_f}\right) = \ln\left(\frac{100}{100 - \%RA}\right) \tag{3}$$

where A_f is the cross-sectional area at fracture and A_0 is the original cross-sectional area. Values of *K* and *n* were obtained according to the ASTM Standard E646 [6] from a least squares fit of true stress versus true plastic strain data in log–log scale. A summary of the monotonic tensile properties is provided in Table 2.

Midlife hysteresis loop data from the fatigue tests were used to determine the steady-state or stable cyclic deformation properties. These consisted of the cyclic strength coefficient, K', cyclic strain hardening exponent, n', and cyclic yield strength, YS'. Values of K' and n' were obtained from a least squares fit of true stress amplitude, $\Delta\sigma/2$, versus true plastic strain amplitude, $\Delta\varepsilon_p/2$, data in log–log scale. These properties are often used to characterize the cyclic deformation curve by a Ramberg–Osgood type equation:

$$\frac{\Delta\varepsilon}{2} = \frac{\Delta\varepsilon_e}{2} + \frac{\Delta\varepsilon_p}{2} = \frac{\Delta\sigma}{2E} + \left(\frac{\Delta\sigma}{2K'}\right)^{1/n'} \tag{4}$$

The cyclic yield strength is analogous to the monotonic yield strength at 0.2% offset.

The cyclic stress–strain curve can be vastly different from the monotonic stress–strain curve. A superimposed plot of the monotonic and cyclic stress–strain curves for SAE 1090 steels (material ID: E) is provided in Fig. 2. As shown in this figure, these high strength steels all cyclic soften. The differences between the cyclic curves are, however, less than the corresponding monotonic curves. The deformation curves of the 1090 steel series are shown since several of these steels exhibit the best overall fatigue resistance, as discussed in the next section. A summary of the cyclic deformation properties of all materials tested is included in Table 2.

Table 2
Summary of monotonic tensile and strain-controlled deformation and fatigue properties

Material ID	E (GPa)	YS/YS' (Mpa/MPa)	S_u (MPa)	%EL	%RA	K/K' (MPa/MPa)	n/n'	σ_f/σ_f' (MPa/MPa)	ϵ_f/ϵ_f'	b	c	S_f (MPa)	N_t (cycles)
A1	216	457/424	771	40%	57%	1394/1515	0.216/0.205	1207/1168	0.85/0.257	−0.097	−0.464	286	18764
A2	227	814/591	925	32%	59%	1205/1277	0.074/0.124	1405/1127	0.88/0.309	−0.066	−0.514	433	5034
A3	220	418/405	695	35%	53%	1287/1448	0.217/0.205	999/1117	0.76/0.264	−0.096	−0.462	276	24439
A4	217	602/481	802	32%	54%	1199/1254	0.126/0.154	1228/1080	0.77/0.361	−0.079	−0.508	342	10845
A5	214	450/447	725	32%	49%	1321/1467	0.207/0.191	1087/1255	0.68/0.430	−0.102	−0.529	287	11606
A6	215	610/487	797	34%	58%	1244/1270	0.141/0.154	1243/1162	0.88/0.534	−0.086	−0.555	332	9045
A7	220	493/481	789	30%	47%	1379/1441	0.187/0.177	1117/1326	0.64/0.602	−0.103	−0.581	296	7608
B1	201	331/342	582	44%	54%	1106/1340	0.259/0.220	898/1043	0.77/0.309	−0.107	−0.481	222	27248
B2	219	359/358	652	38%	53%	1186/1420	0.219/0.222	1051/1004	0.76/0.202	−0.098	−0.440	241	32782
B3	219	410/364	649	45%	67%	1183/1330	0.221/0.208	1197/1009	1.10/0.225	−0.097	−0.460	248	31485
C1	205	475/424	783	39%	55%	1576/1416	0.235/0.194	/1622	0.80/0.515	−0.135	−0.548	228	12496
C2	205	475/469	906	29%	42%	1924/950	0.204/0.114	/1044	0.54/0.513	−0.083	−0.557	315	8378
D1	211	465/427	821	43%	50%	1819/1673	0.274/0.220	/989	0.68/0.433	−0.126	−0.512	159	62548
D2	203	460/523	829	18%	34%	1313/1292	0.163/0.146	/1094	0.42/0.309	−0.075	−0.502	369	6513
D3	203	2000/1796	2360	17%	15%	2837/3538	0.048/0.109	/3492	0.16/1.870	−0.109	−1.040	717	77
E1	203	735/545	1090	9%	14%	1765/1611	0.158/0.174	/1310	0.15/0.250	−0.091	−0.496	350	4199
E2	203	950/730	1388	14%	25%	1980/1663	0.080/0.133	/1945	0.29/2.580	−0.106	−0.777	417	2104
E3	217	650/627	1147	67%	22%	1895/1873	0.165/0.176	/1878	0.24/0.700	−0.120	−0.600	328	4739
E4	203	760/645	1251	7%	14%	2757/1835	0.264/0.168	/1928	0.15/0.734	−0.120	−0.642	337	2090
E5	203	765/615	1124	18%	38%	1535/1653	0.100/0.159	/1547	0.47/1.570	−0.093	−0.683	401	4224

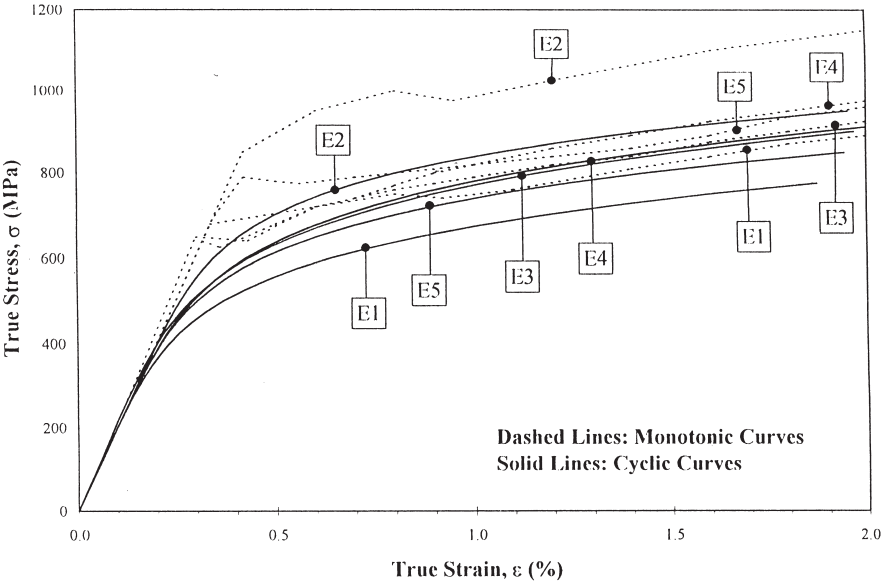

Fig. 2. Monotonic and cyclic stress–strain curves for SAE 1141 steels.

3.2. Strain-controlled fatigue behavior and properties

The fatigue strength coefficient, σ_f', and exponent, b, were obtained from a least squares fit of true stress amplitude, $\Delta\sigma/2$, versus reversals to failure, $2N_f$, data in log–log scale. The fatigue ductility coefficient, ε_f', and exponent, c, were obtained from a similar plot of the true plastic strain amplitude, $\Delta\varepsilon_p/2$, versus reversals to failure, $2N_f$. A typical strain–life curve is shown in Fig. 3. It should be noted that significant variations in these properties for a given material can exist, depending on the curve-fitting techniques employed. These variations mainly result from the method of determining elastic and plastic strains, sensitivity of the fittings and obtained properties to the value of modulus of elasticity used, and selection of dependent versus independent variables in performing least squares fits. Elastic and plastic strains can either be directly measured from the hysteresis loops, or calculated from $\Delta\varepsilon_e/2=\Delta\sigma/2E$ and $\Delta\varepsilon_p/2=\Delta\varepsilon/2-\Delta\sigma/2E$. The elastic modulus used for the calculations can either be measured from monotonic tension tests, or from the hysteresis loops in fatigue tests. In fitting the experimental data to obtain material cyclic properties, fatigue life should be treated as the dependent variable (i.e. y value in an x–y plot of spreadsheet data). The variability in properties based on the different aforementioned curve-fitting techniques is discussed in [7].

A superimposed plot of strain–life curves for all materials is provided in Fig. 4. Due to the large number of curves in this plot, references for the end points are provided on the left and right sides of the strain–life curves. For the low cycle fatigue region the hierarchical order of the end point references indicates which materials are able to endure more plastic deformation. Conversely, for the high cycle fatigue region the hierarchical order of the end point references indicates which materials are able to endure more elastic deformation. Therefore, materials that occur near the top of both these reference lists are considered "tough" materials because they excel in both life regions. For example, the SAE 1090(M) steels (E2 and E5 steels) with pearlite/martensite microstructure, have ultimate tensile strengths of 1388 MPa and 1124 MPa, respectively, and ductility as measured by percent reduction in area of 25% and 38%, respectively. These steels are, therefore, tough steels and show superior low cycle as well as high cycle fatigue resistances.

A variation of the strain–life plot can be used to evaluate the notched fatigue resistance of materials. The most widely used method for estimating notch stress and strain is Neuber's rule. The general form of this relationship for cyclic loading is given by:

$$\sqrt{\left(\frac{\Delta\sigma}{2}\right)\left(\frac{\Delta\varepsilon}{2}\right)E}=K_t\left(\frac{\Delta S}{2}\right) \tag{5}$$

where $\Delta\sigma/2$ and $\Delta\varepsilon/2$ are the notch root stress and strain amplitudes, $\Delta S/2$ is the nominal stress amplitude, and K_t is the elastic stress concentration factor. Neuber's parameter, which is represented by the left side of Eq. (5), is plotted in Fig. 5 for all materials. The hierarchical order of the end point references in Fig. 5 indicates the notched fatigue resistance of the materials for the different life regions. Materials that occur near the top of both reference lists indicate high notched fatigue resistance over the entire life range.

Representative macroscopic fatigue crack growth and final fracture surface features can be seen from Fig. 6

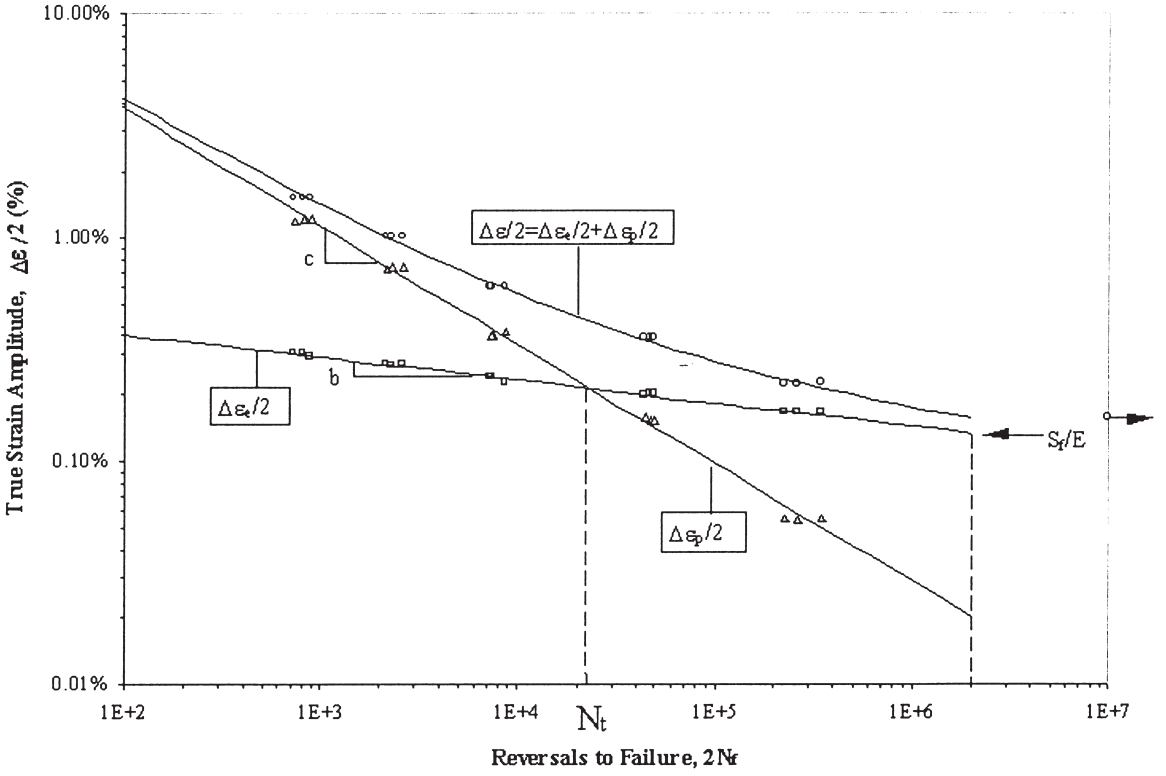

Fig. 3. Example of true strain amplitude vs. reversals to failure (SAE 1141 VFG steel).

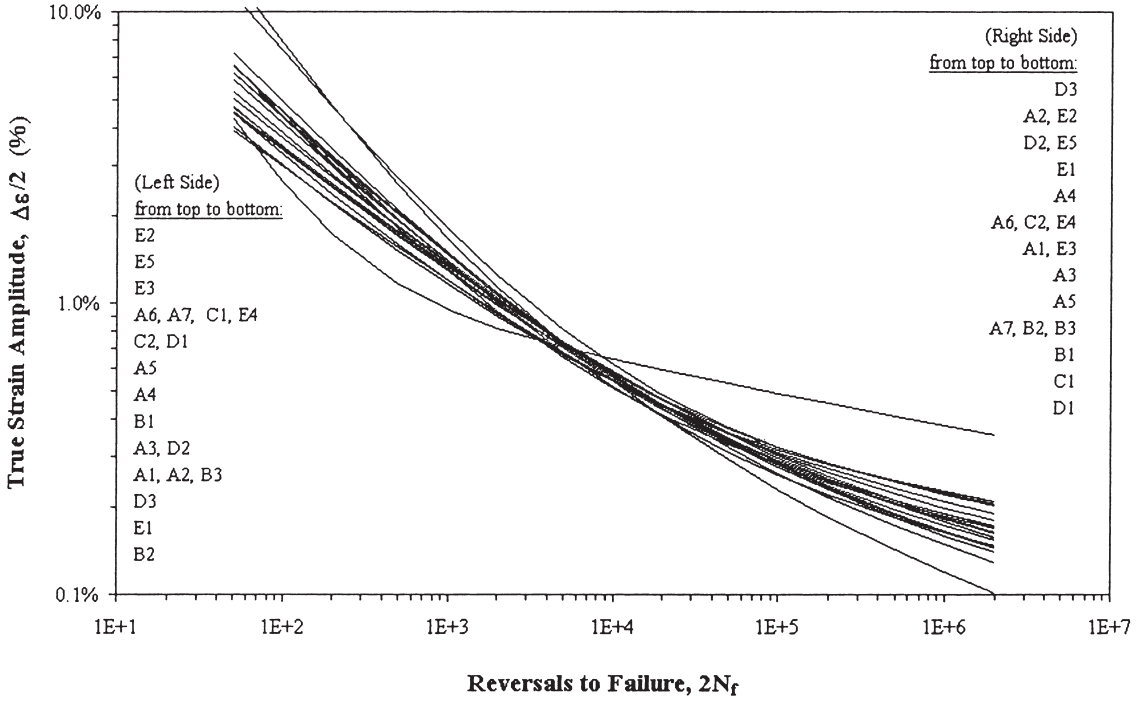

Fig. 4. Superimposed plot of true strain amplitude vs. reversals to failure for all materials.

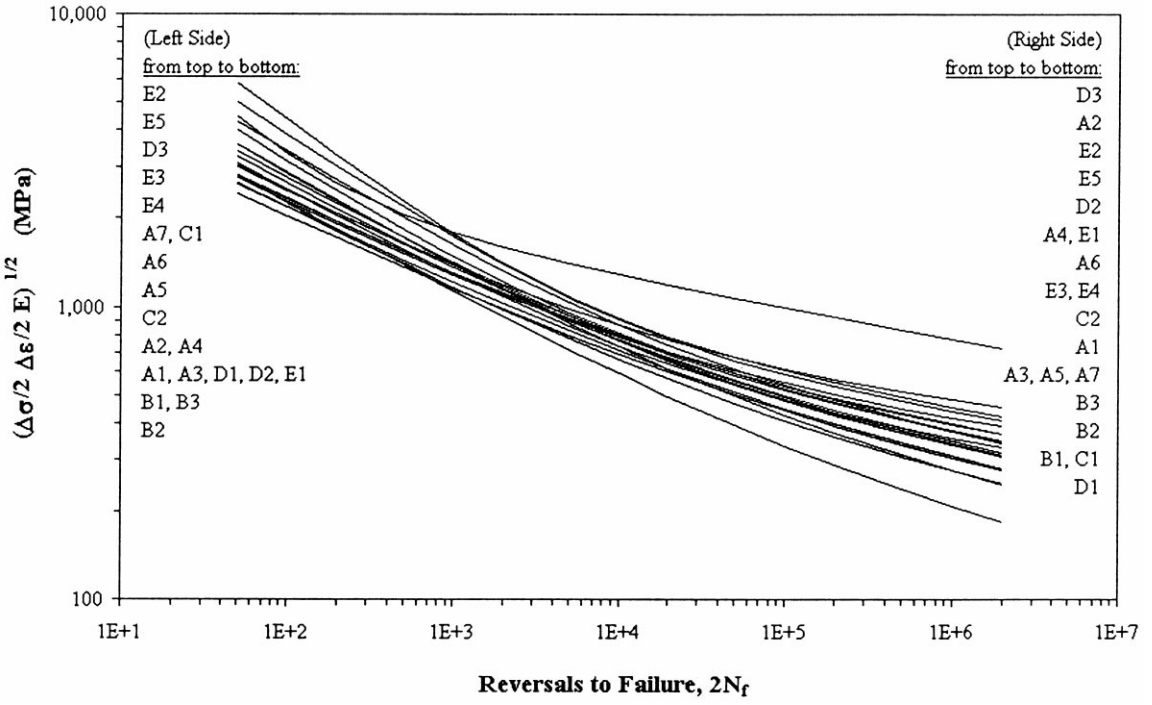

Fig. 5. Superimposed plot of Neuber's parameter vs. reversals to failure for all materials.

for the Q and T A2 steel (Fig. 6(a) and (b)) and the normalized A3 steel (Fig. 6(c) and (d)). Figure 6 (a) and (c) are from low cycle fatigue (LCF) tests, whereas Fig. 6(b) and (d) are from high cycle fatigue (HCF) tests. The final fracture surfaces represented by the darker regions in each figure are rougher than the relatively smooth fatigue crack growth regions (lighter color regions). Also, LCF crack growth regions (Fig. 6(a) and (c)) are somewhat rougher than HCF crack growth regions (Fig. 6(b) and (d)), indicating higher crack growth rates. Fatigue crack growth regions in HCF tests occupy a larger portion of the fracture surface, compared to fracture surfaces from LCF tests, indicating longer cracks sustained at lower loads. "Beach marks" are absent from the fracture surfaces, indicating uniform straining throughout the cracking phase. A "sunrise" pattern can be seen in Fig. 6(b), as the crack grew on slightly different levels or planes, simultaneously. The center of the rays point to the crack nucleation site. Typical microscopic features of the fracture surfaces can be seen from the fractographs shown in Fig. 7 for the Q and T A2 steel (Fig. 7(a)) and the normalized A3 steel (Fig. 7(b)). These SEM fractographs show the fatigue crack growth region, indicating cracking and decohesion of inclusions. Both materials sustained large plastic deformations, resulting in ductile fracture.

Table 2 includes a summary of the strain-controlled fatigue properties. As may be seen in this table, the fatigue strength exponent, b, ranged from -0.066 to -0.135, with an average value of -0.10, while the fatigue ductility exponent, c, ranged from -0.44 to -1.04, with an average value of -0.57. The fatigue limit, S_f, and the transition fatigue life, N_t, are also given in Table 2. The fatigue limit was calculated from Eq. (1), using $N_f=10^6$ cycles. The transition fatigue life indicates when a material will experience equal amounts of elastic and plastic strains, as shown in Fig. 3. It can be obtained by setting equal the elastic strain amplitude, $\Delta\varepsilon_e/2=\sigma_f'/E(2N_f)^b$, and the plastic strain amplitude, $\Delta\varepsilon_p/2=\varepsilon_f'(2N_f)^c$, resulting in the following equation:

$$N_t=\frac{1}{2}\left(\frac{\sigma_f'}{\varepsilon_f' E}\right)^{1/(c-b)}. \quad (6)$$

4. Correlations among tensile data and fatigue properties

As mentioned previously, it is often desirable to estimate fatigue behavior of a material from easily and quickly obtainable material properties such as hardness and tensile data, with a reasonable degree of accuracy. Therefore, many correlations among the monotonic tensile data and fatigue properties of materials have been proposed. In this section, the data presented in the previous section are used to evaluate some of the more commonly used correlations, as well as to develop a simple method for estimating material strain–life curve. In addition to the 20 steels from this study, data from 49 other steels were selected from the American Society for

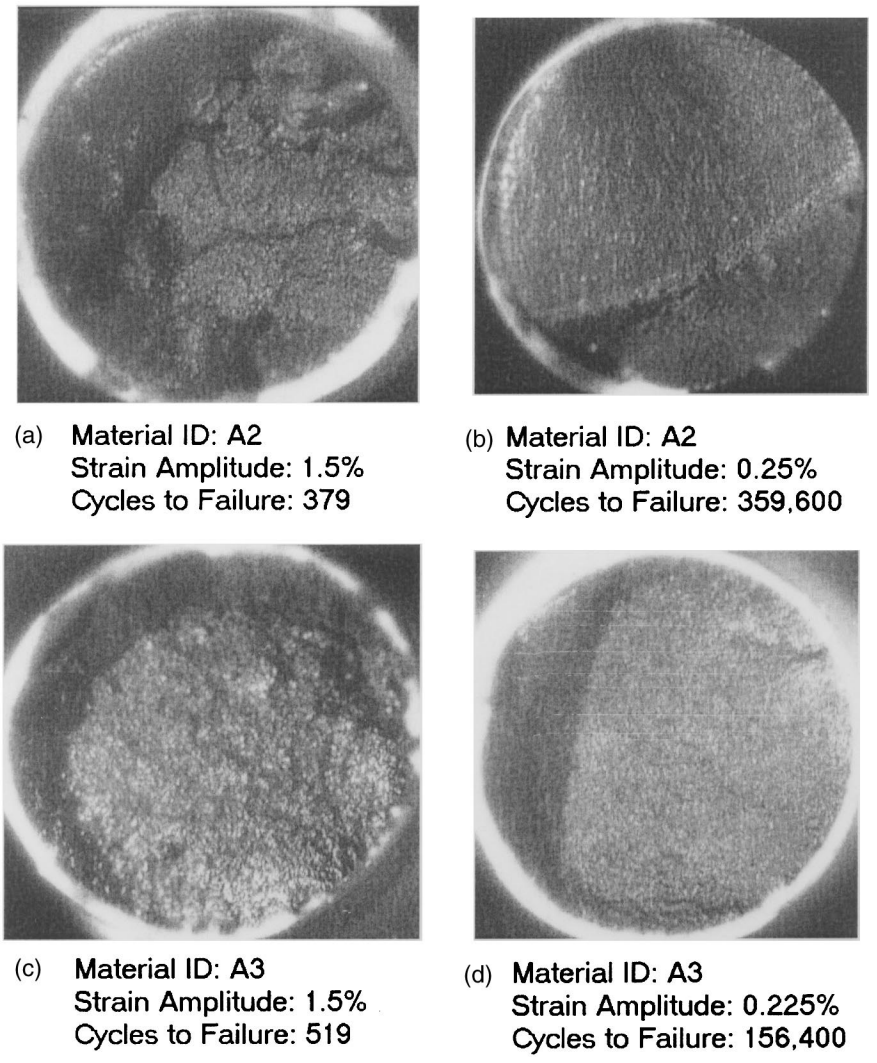

Fig. 6. Representative macroscopic fractographs at 15×.

Metals (ASM) reference book [1] to evaluate correlations among the monotonic and fatigue properties. These steels include plain carbon steels, resulfurized carbon steels, chromium–molybdenum steels, nickel–chromium–molybdenum steels, chromium steels, silicon–manganese steels, high strength low-alloy steels, and alloy steel pressure vessel plate steels. By using a total of 69 steels, Brinell hardness, *HB*, ranged from 80 to 660, ultimate tensile strength, S_u, ranged from 345 MPa to 2585 MPa, and percent reduction in area, %*RA*, ranged from 11% to 80%. Therefore, a broad range of steels is used for the correlations.

4.1. Correlations among tensile strength, hardness, fatigue limit, and transition life

A commonly used approximation of the ultimate tensile strength, S_u, from Brinell hardness, *HB*, for low and medium strength carbon and alloy steels is represented by a linear relationship as:

$$S_u \cong 3.45HB \text{ (MPa)} \quad (7)$$

A plot of ultimate tensile strength vs. Brinell hardness is provided in Fig. 8. It may be seen from this figure that the approximation from Eq. (7) agrees well with experimental data for $HB<350$. A least squares fit using a second-order polynomial results in the following correlation with $R^2=0.96$:

$$S_u = 0.0012(HB)^2 + 3.3(HB) \text{ (MPa)} \quad (8)$$

For steels with hardness less than 500 HB, the fatigue limit, S_f, has been suggested to be estimated from the Brinell hardness as follows [8]:

$$S_f \cong 1.72HB \text{ (MPa)} \quad (9)$$

A plot of the fatigue limit vs. Brinell hardness is provided in Fig. 9. As can be seen, there is a poor agreement between the data and the predictions obtained from Eq. (9). A linear least squares fit through the data with $R^2=0.91$ results in the following relationship:

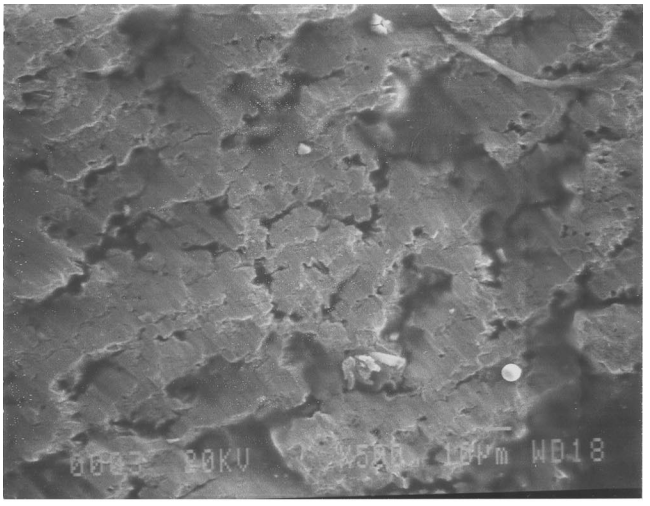

(a)

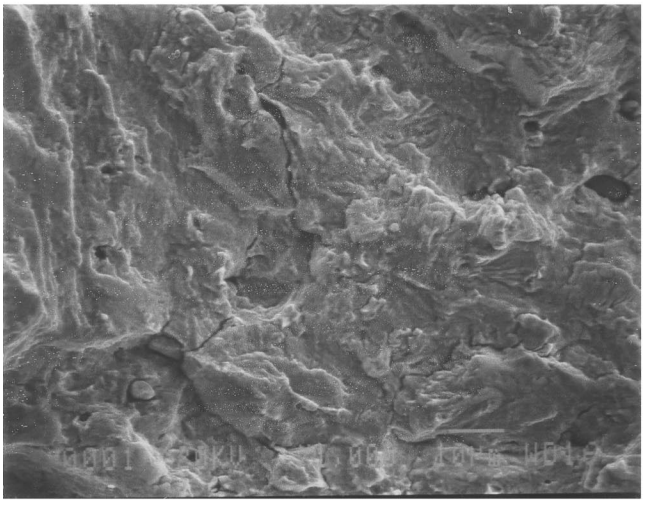

(b)

Fig. 7. Representative SEM fractographs. (a) SAE 1141 Q&T steel (A2) fatigue fracture surface ε_a=1.5% at 500X. (b) SAE 1141 normalized steel (A3) fatigue fracture surface (ε_a=0.23%) at 1000X.

$$S_f = 1.43HB \text{ (MPa)} \tag{10}$$

The fatigue limit can also be estimated from the ultimate tensile strength. An approximation that is often used for steels is as follows:

$$\begin{aligned} S_f &\cong 0.5\, S_u \quad \text{for } S_u \leq 1400 \text{ MPa} \\ S_f &\cong 700 \text{ MPa} \quad \text{for } S_u > 1400 \text{ MPa} \end{aligned} \tag{11}$$

The reason for a constant value of fatigue limit for steels with S_u>1400 MPa is thought to be due to the role of inclusions [9]. At such high strengths, fatigue limit becomes more dependent on the size and dispersion of inclusions and other impurities. In Fig. 10, a plot of the fatigue limit vs. ultimate tensile strength is provided. It can be seen from this figure that there is a large amount of scatter in the data and that predictions based on Eq. (11) have poor agreement with the data and are nonconservative for most of the steels. It should be mentioned that traditionally most fatigue limit data are obtained from rotating bending fatigue tests, whereas here the values are from axial fatigue tests. In axial fatigue tests, lower strengths are often obtained due to reasons such as higher probability of defects associated with larger stressed volume and bending resulting from specimen misalignment. A fit through all of the data in Fig. 10 and a fit through data having $S_u \leq 1400$ MPa were found to be equivalent. Therefore, a correlation with R^2=0.86 was obtained as follows:

$$S_f = 0.38\, S_u \tag{12}$$

The transition fatigue life, N_t, indicates when a material will experience equal amounts of cyclic elastic and plastic strains. Knowing the transition life for a material allows plastic and elastic strain dominated life regimes to be identified and the appropriate life prediction approach to be selected accordingly. Landgraf [10] has shown that there is a dependence of transition life on Brinell hardness for steels. Since hardness varies inversely with ductility, the transition life decreases as the hardness increases. The relationship shown by Landgraf may be expressed as follows:

$$\log(2N_t) = 6.126 - 0.0083\, HB \tag{13}$$

A semi-log plot of transition life vs. Brinell hardness is shown in Fig. 11. It may be seen from this figure that the correlation obtained from a least squares fit of the data is in close agreement with predictions from Eq. (13). This correlation with R^2=0.89 is given by:

$$\log(2N_t) = 5.755 - 0.0071\, HB. \tag{14}$$

4.2. Approximations of strain–life properties

The fatigue strength coefficient, σ_f', is analogous to the true fracture strength, σ_f, obtained from a tensile test. Several relations for estimating fatigue strength coefficient from true fracture strength have been proposed, with estimates ranging from 0.92 σ_f to 1.15 σ_f. As can be seen from Table 2, there is no strong correlation between σ_f' and σ_f. The fatigue strength coefficient was found to be more dependent upon the Brinell hardness and ultimate tensile strength of the steel. Plots of fatigue strength coefficient vs. Brinell hardness and ultimate tensile strength are shown in Fig. 12 and Fig. 13, respectively. These figures show relatively good linear least squares fits for the data, represented by:

$$\sigma_f' = 4.25\, HB + 225 \text{ (MPa)} \tag{15}$$

$$\sigma_f' = 1.04\, S_u + 345 \text{ (MPa)} \tag{16}$$

The approximation from the literature shown in Fig. 13

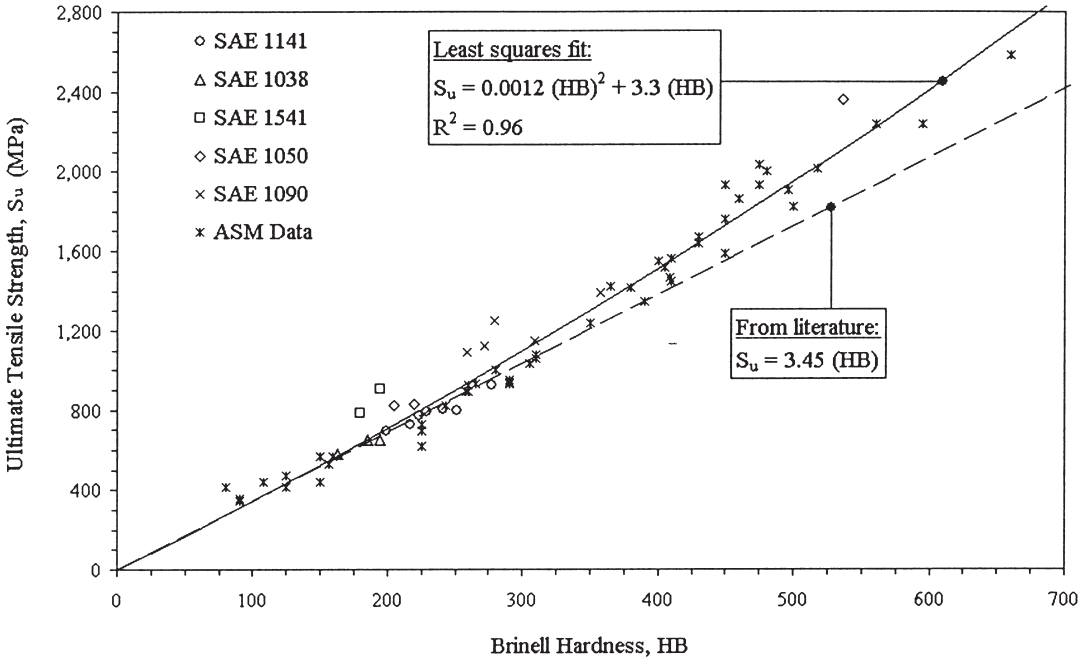

Fig. 8. Ultimate tensile strength vs. Brinell hardness.

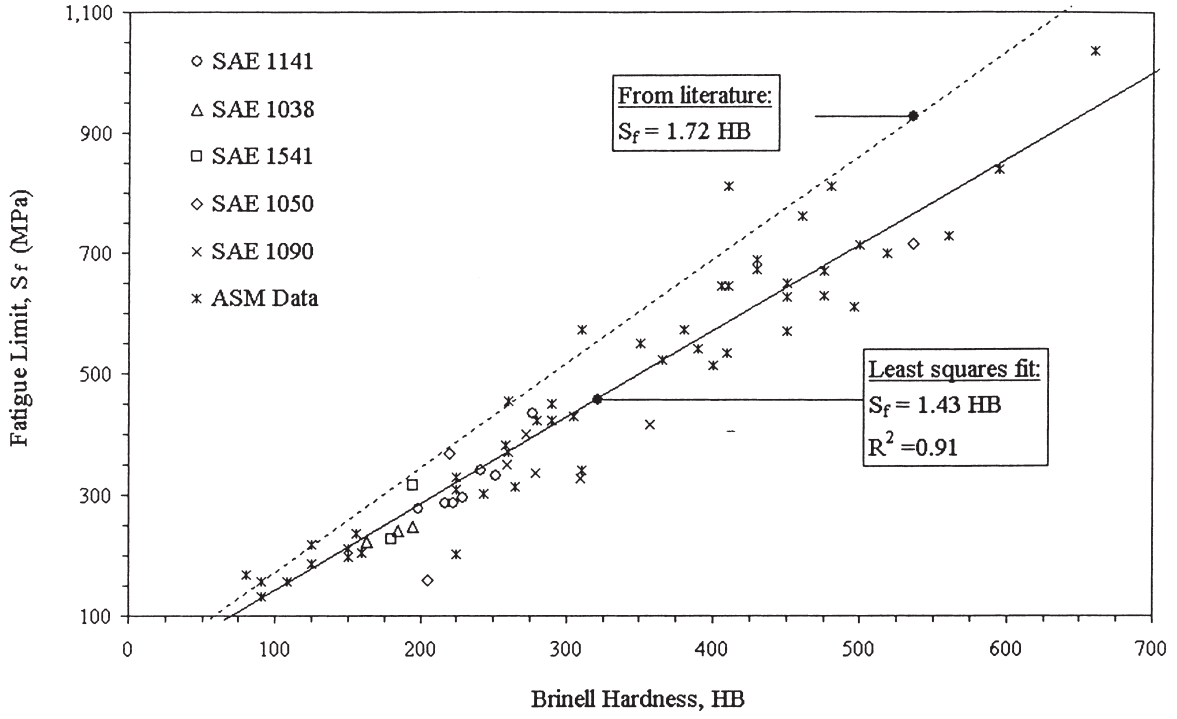

Fig. 9. Fatigue limit vs. Brinell hardness.

is in very close agreement with the linear fit represented by Eq. (16).

The fatigue ductility coefficient, ε_f', is thought to be of the same order as the true fracture ductility, ε_f, obtained from a tensile test. The proposed relations in the literature predict the fatigue ductility coefficient to be from 0.15 ε_f to 1.1 ε_f. As can be seen from Fig. 14, there is no clear correlation between ε_f' and ε_f. Therefore, using the true fracture ductility to approximate the fatigue ductility coefficient can result in significant error.

As shown by Morrow [11] through energy arguments, a relationship can be derived between the cyclic strain

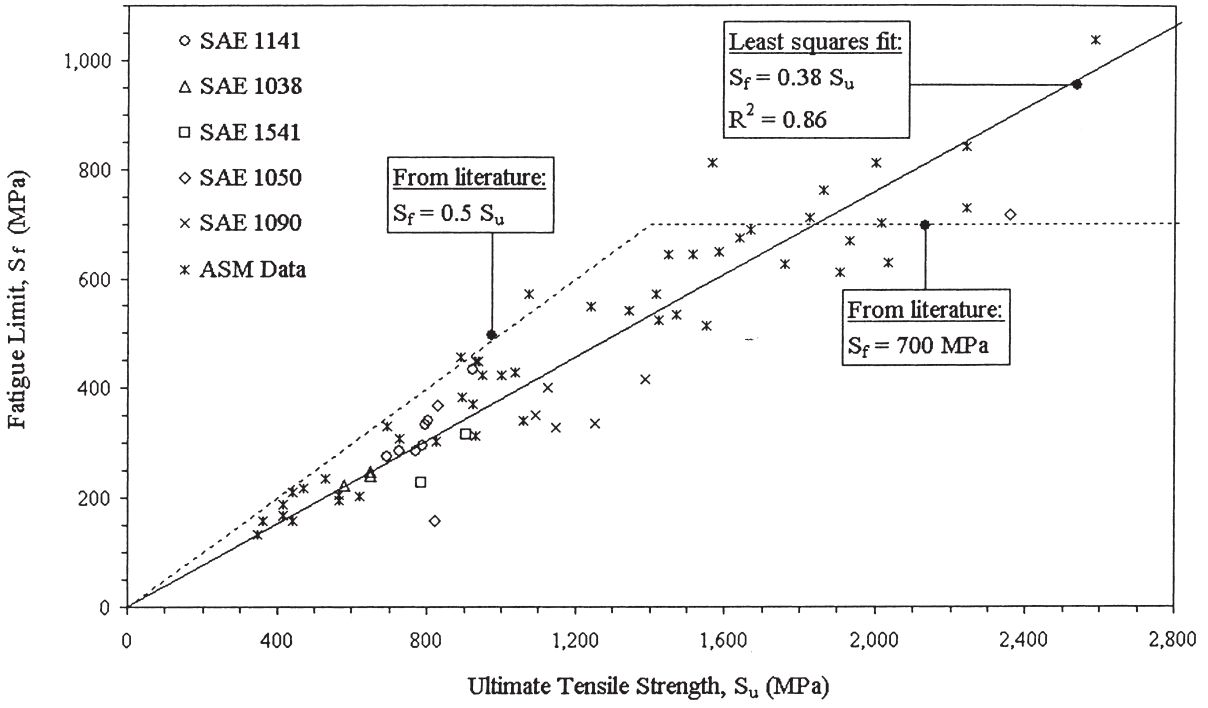

Fig. 10. Fatigue limit vs. ultimate tensile strength.

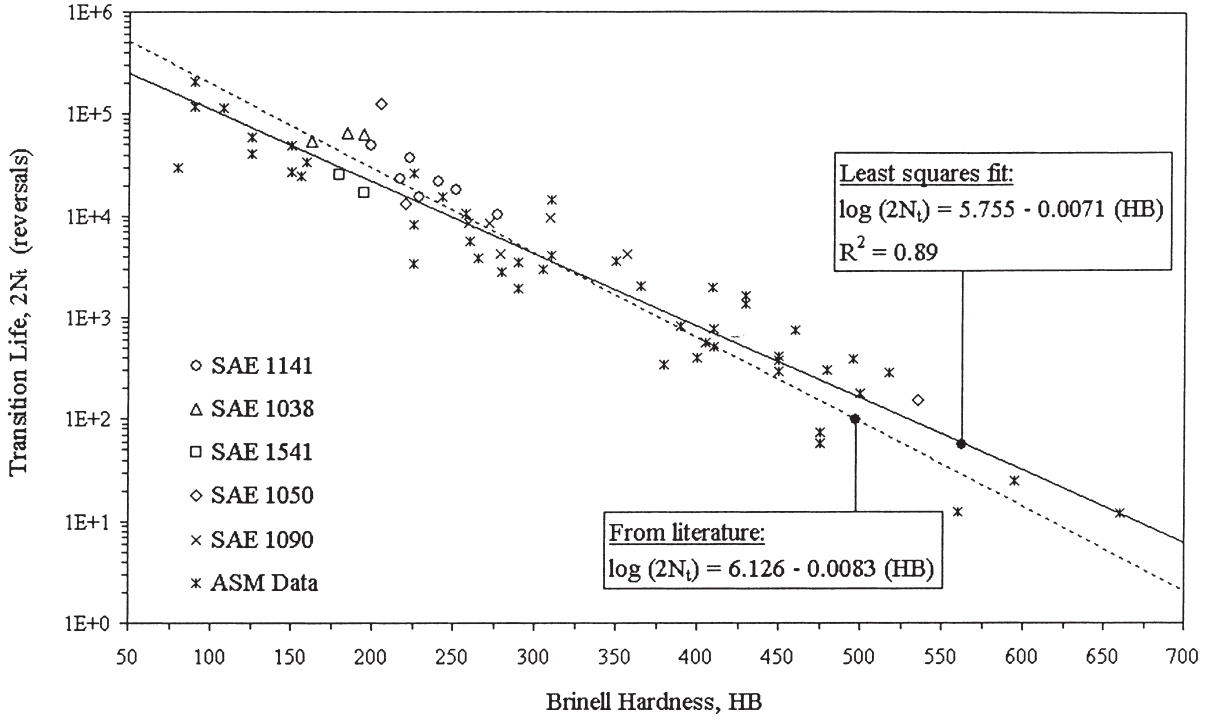

Fig. 11. Transition life vs. Brinell hardness.

hardening exponent, n', and the fatigue strength and ductility exponents (b and c). The relationships that follow were developed from a variety of metals and illustrated using data for SAE 4340 steel [11]:

$$b=\frac{-n'}{1+5n'},\quad c=\frac{-1}{1+5n'} \tag{17}$$

These equations, however, resulted in poor agreements

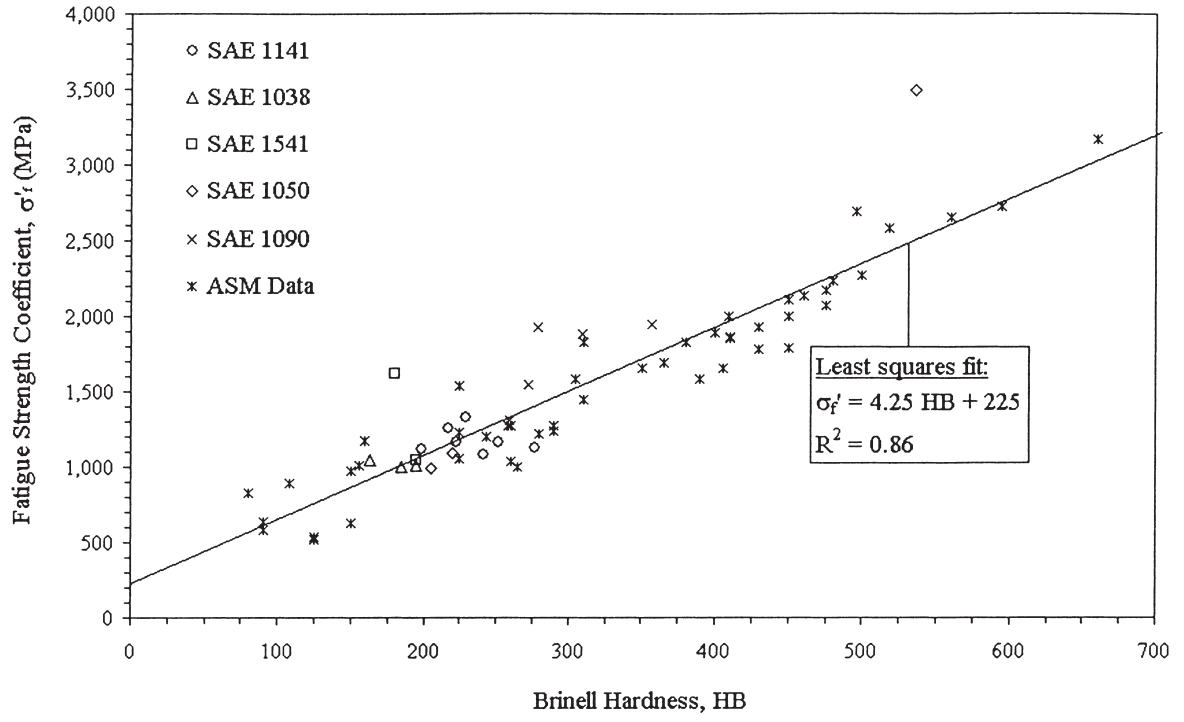

Fig. 12. Fatigue strength coefficient vs. Brinell hardness.

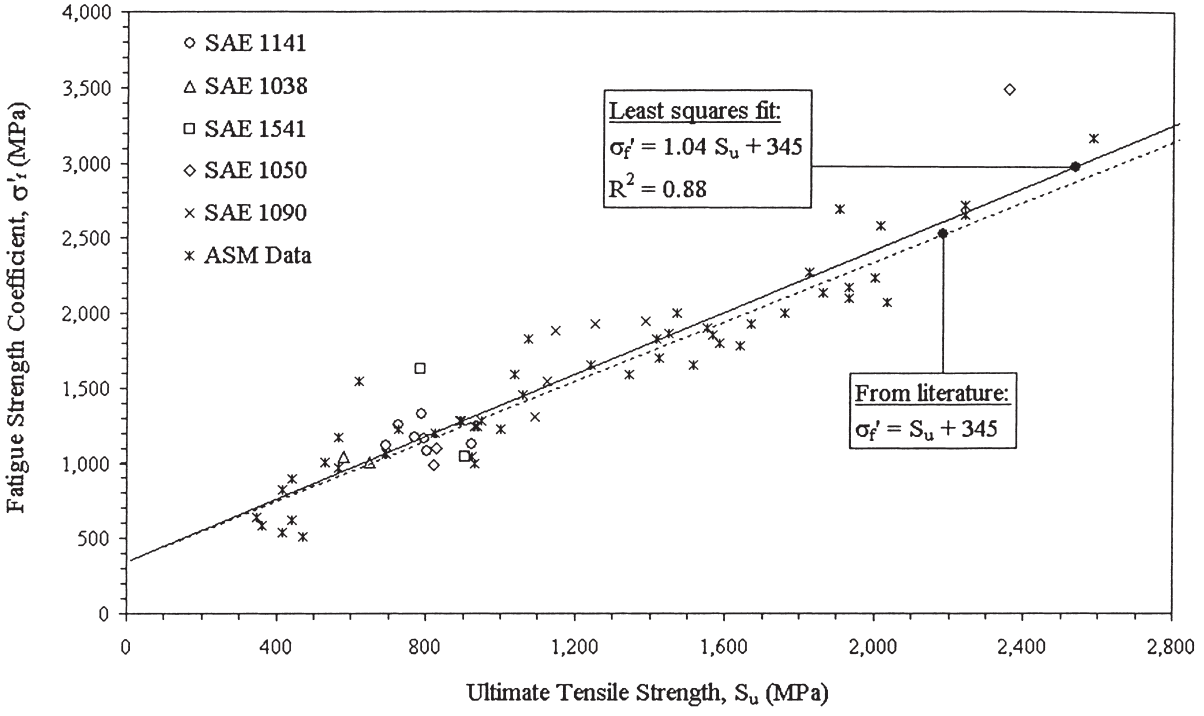

Fig. 13. Fatigue strength coefficient vs. ultimate tensile strength.

with the data from the 20 steels in this study. Values of n' for the ASM data were not available. The fatigue strength exponent, b, ranged from -0.057 to -0.140 with an average value of -0.09, and the fatigue ductility exponent, c, ranged from -0.39 to -1.04 with an average value of -0.60.

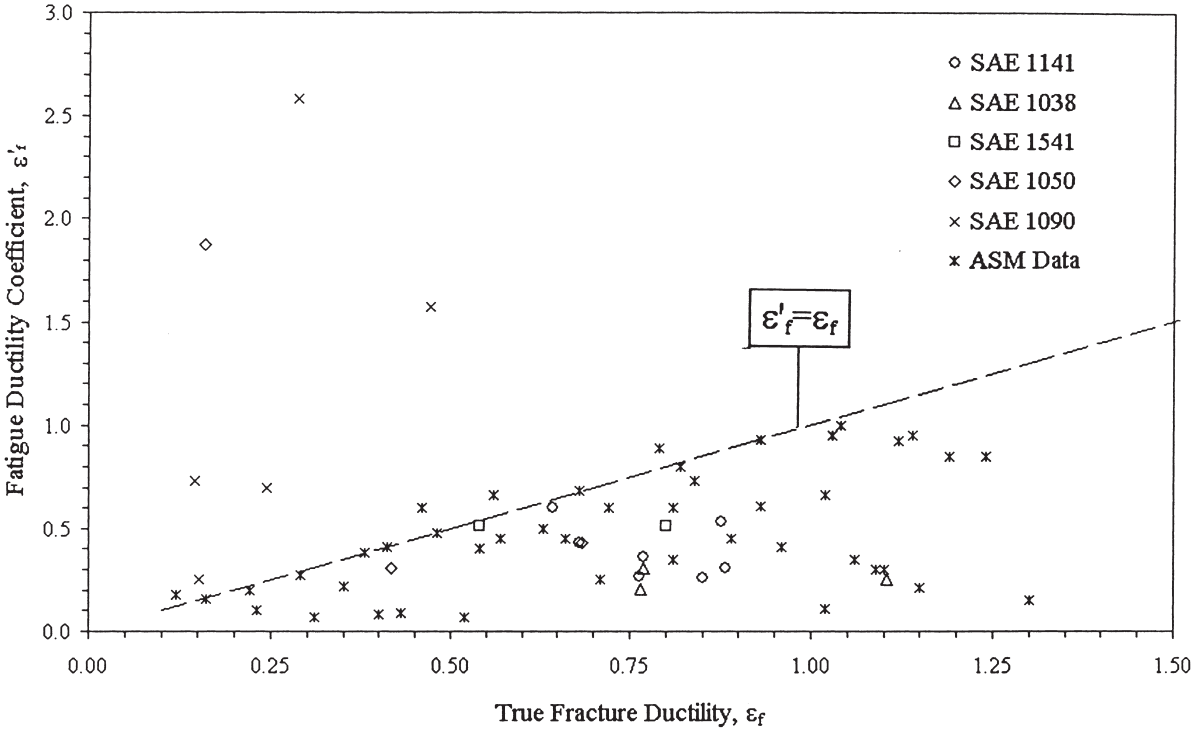

Fig. 14. Fatigue ductility coefficient vs. true fracture ductility.

4.3. Approximations of the strain–life curve from tensile properties

Several researchers have developed empirical relations to predict strain–life fatigue behavior using monotonic tensile properties. Some of these relations provide good approximations for a variety of materials. In a study conducted by Park and Song [12], six such methods were evaluated and compared. These consisted of the Universal Slopes and the Four-Point Correlation methods by Manson [13], the Modified Universal Slopes method by Muralidharan and Manson [14], the Uniform Material method by Bäumel and Seeger [15], the Modified Four-Point Correlation method by Ong [16], and the method proposed by Mitchell et al. [8]. A total of 138 materials were used in the study including unalloyed steels, low-alloy steels, high-alloy steels, aluminum alloys, and titanium alloys, with low-alloy steels providing the most data. Amongst the correlations compared, those proposed by Muralidharan and Manson [14], Bäumel and Seeger [15], and Ong [16] yielded good predictions according to Park and Song. The Modified Universal Slopes method was concluded to provide the best correlation. This method is given by:

$$\frac{\Delta\varepsilon}{2}=0.623\left(\frac{S_u}{E}\right)^{0.832}(2N_f)^{-0.09} \tag{18}$$

$$+0.0196(\varepsilon_f)^{0.155}\left(\frac{S_u}{E}\right)^{-0.53}(2N_f)^{-0.56}$$

Another study that compared correlations for estimating fatigue properties from monotonic tensile data is by Ong [17]. In that study, the ASM data for 49 steels were used and the correlations compared were the modified and original versions of the Four-Point Correlation method, the Original Universal Slopes method, and the Mitchell et al. method. The best predictions were shown to result from the Modified Four-Point Correlation method.

4.4. Proposed approximation of strain–life curve from hardness and modulus of elasticity

A new method for estimation of the strain–life curve is proposed. This method evolved from a careful examination of the previous methods with the goal of deriving a strain–life approximation equation that required the least amount and the most common material properties. These properties are hardness and modulus of elasticity.

To derive this relationship, each of the four strain–life fatigue constants was first estimated based on the data obtained from the 69 steels used in this study. The fatigue strength coefficient, σ'_f, showed a relatively strong correlation with hardness as indicated by Fig. 12 and represented by Eq. (15). The fatigue ductility coefficient, ε'_f, is found from Eq. (6) in terms of the transition fatigue life, N_t, as:

$$\varepsilon'_f=\frac{\sigma'_f(2N_t)^b}{E(2N_t)^c} \tag{19}$$

where the nominator is the transition fatigue strength, S_t, corresponding to N_t, $S_t=\sigma_f'(2N_t)^b$. A strong correlation (with R^2=0.97) was found between S_t and hardness, *HB*, represented by the following relation:

$$S_t=0.004\,(HB)^2+1.15\,(HB) \tag{20}$$

Substituting the right side of Eq. (20) for the nominator of Eq. (19), and using Eq. (14) to relate N_t in the denominator of Eq. (19) to hardness, *HB*, results in:

$$\varepsilon_f'=\frac{0.004(HB)^2+1.15\,HB}{E[10^{(5.755-0.0071\,HB)}]^{-0.56}} \tag{21}$$

A simpler second-order polynomial represents Eq. (21) with a very close agreement for $150<HB<700$ as follows:

$$\varepsilon_f'=\frac{0.32(HB)^2-487(HB)+191000}{E} \tag{22}$$

The fatigue strength exponent, *b*, ranged from −0.057 to −0.140 with the average value of −0.09. This average value is the same as the constant value used by the Modified Universal Slopes method given by Eq. (18). Therefore, the fatigue strength exponent, *b*, was estimated to have a constant value of −0.09. The fatigue ductility exponent, *c*, ranged from −0.39 to −1.04 with the average value of −0.60. However, since this value is close to that in the Modified Universal Slopes method, the fatigue ductility exponent, *c*, was also approximated as a constant value of −0.56.

After substituting the approximated fatigue constants into the strain–life equation (Eq. (2)), the final form of the proposed correlation is as follows:

$$\frac{\Delta\varepsilon}{2}=\frac{4.25(HB)+225}{E}(2N_f)^{-0.09}+\frac{0.32(HB)^2-487(HB)+191000}{E}(2N_f)^{-0.56} \tag{23}$$

This approximation uses only hardness and modulus of elasticity (in MPa) as inputs for strain–life approximation, both of which are either commonly available, or easily measurable. Eq. (23) provides reasonably accurate predictions for steels with a Brinell hardness larger than 150. As can be seen from this equation, with an increase in hardness the fatigue strength coefficient increases and the fatigue ductility coefficient decreases, which agrees with expectations.

To evaluate prediction capabilities of this method, comparisons were made between this proposed relation and the three methods yielding the best predictions in the study by Park and Song [12] mentioned previously. These three methods consisted of the Modified Universal Slopes method, the Uniform Material method, and the Modified Four-Point Correlation method. For each method, a log–log plot of predicted vs. experimental strain amplitudes was made using data from the 69 steels. Experimental strain amplitude data were obtained from strain–life curve for each material at fatigue lives of 10^3, 10^4, 10^5 and 10^6 reversals. All of the three methods resulted in reasonable predictions, even though some differences existed in different life regimes. As an illustration, the plot for the Modified Universal Slopes method is shown in Fig. 15. For comparison, prediction of strain amplitudes based on the proposed method is shown in Fig. 16. Only strain amplitudes between 0.1% to 1% are shown in these figures in order to illustrate the spread of the data, since this range is usually the practical range of strain–life data. However, all of the calculated data are included for the percentage of data values tabulated in Fig. 15 and Fig. 16. It may be seen that the proposed method results in reasonably accurate and somewhat better predictions of the strain amplitudes. For example, 80% of the predicted strain amplitudes based on the proposed equation are within a factor of ±1.2 of the experimental strain amplitudes, whereas 70% of the predicted strain amplitudes are within this factor for the Modified Universal Slopes method.

For each method, predicted vs. experimental fatigue lives are also plotted. For each steel, fatigue lives were calculated at 1.5%, 1.0%, 0.6%, 0.35%, 0.2%, and 0.15% strain amplitudes. Newton's iterative procedure was used to solve Eq. (2) for life, at each strain amplitude. These plots are shown in Fig. 17 and Fig. 18 for the Modified Universal Slopes and the proposed methods, respectively. The proposed method results in somewhat better and more conservative predictions over the entire fatigue life regime. It should be emphasized, however, that the proposed method only requires hardness and modulus of elasticity of the material.

5. Summary and conclusions

Material data for twenty steels commonly used in the ground vehicle industry were presented and comparisons were made between monotonic deformation, cyclic deformation, and strain-controlled fatigue properties of these steels. The data from these steels in addition to 49 other steels published by the American Society of Metals (ASM) were then used to examine correlations among the various monotonic and fatigue properties. These included relationships among ultimate tensile strength, fatigue limit, fatigue strength coefficient, and hardness, as well as estimation of strain–life fatigue properties and approximation of strain–life curves. Validity of some of the more commonly used methods of estimating fatigue properties found in the literature was evaluated and improvements upon some of these correlations are suggested. Based on the discussions in the preceding sections, the following conclusions can be drawn:

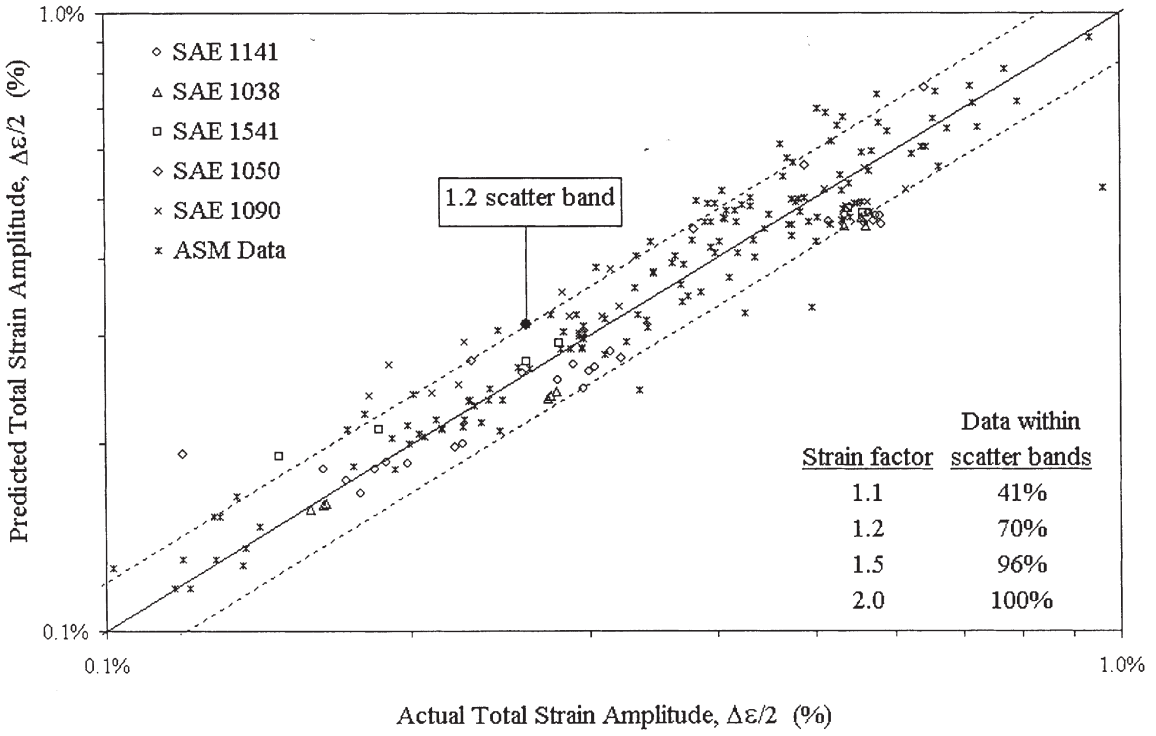

Fig. 15. Prediction of total strain amplitude by the Modified Universal Slopes method.

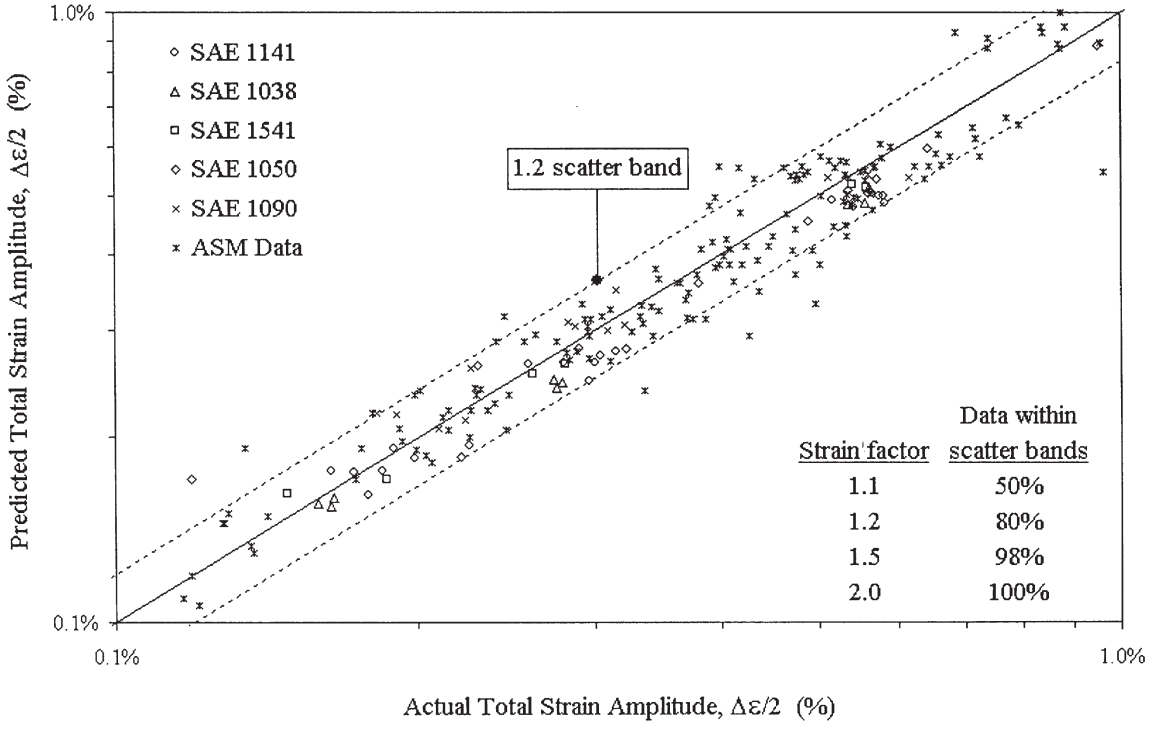

Fig. 16. Prediction of total strain amplitude by the proposed method.

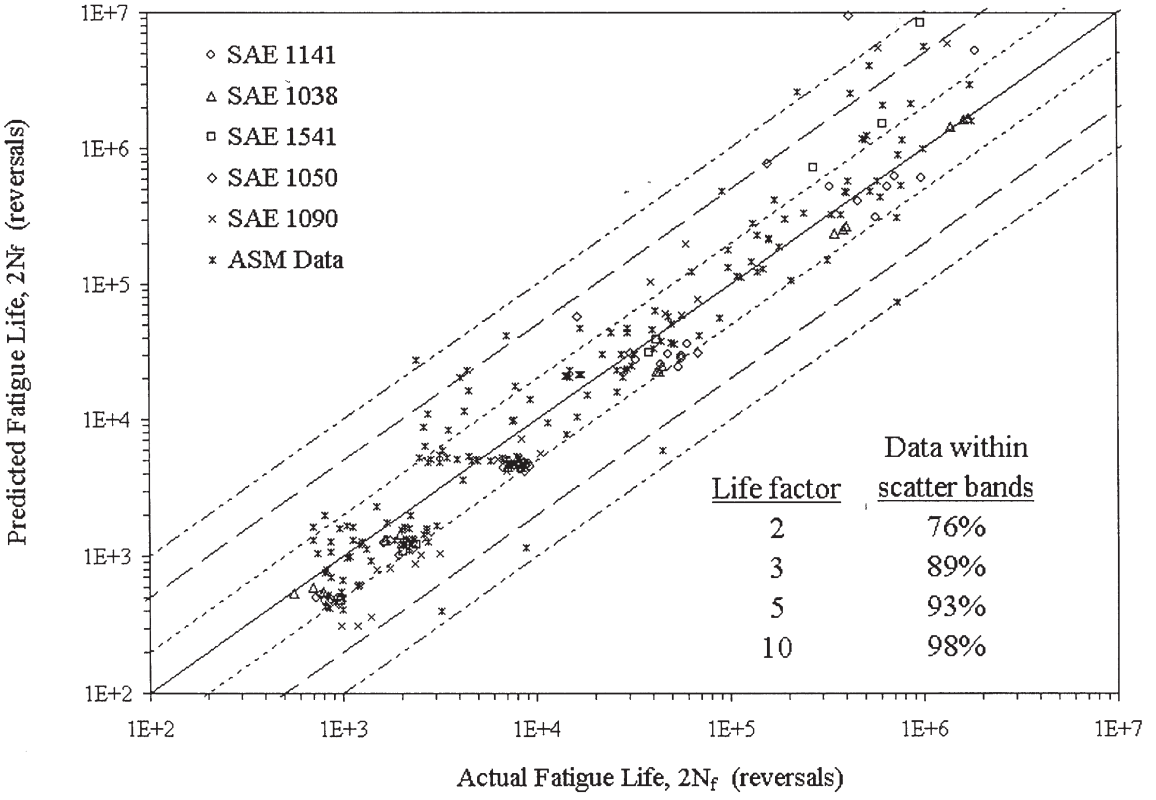

Fig. 17. Prediction of fatigue life by the Modified Universal Slopes method.

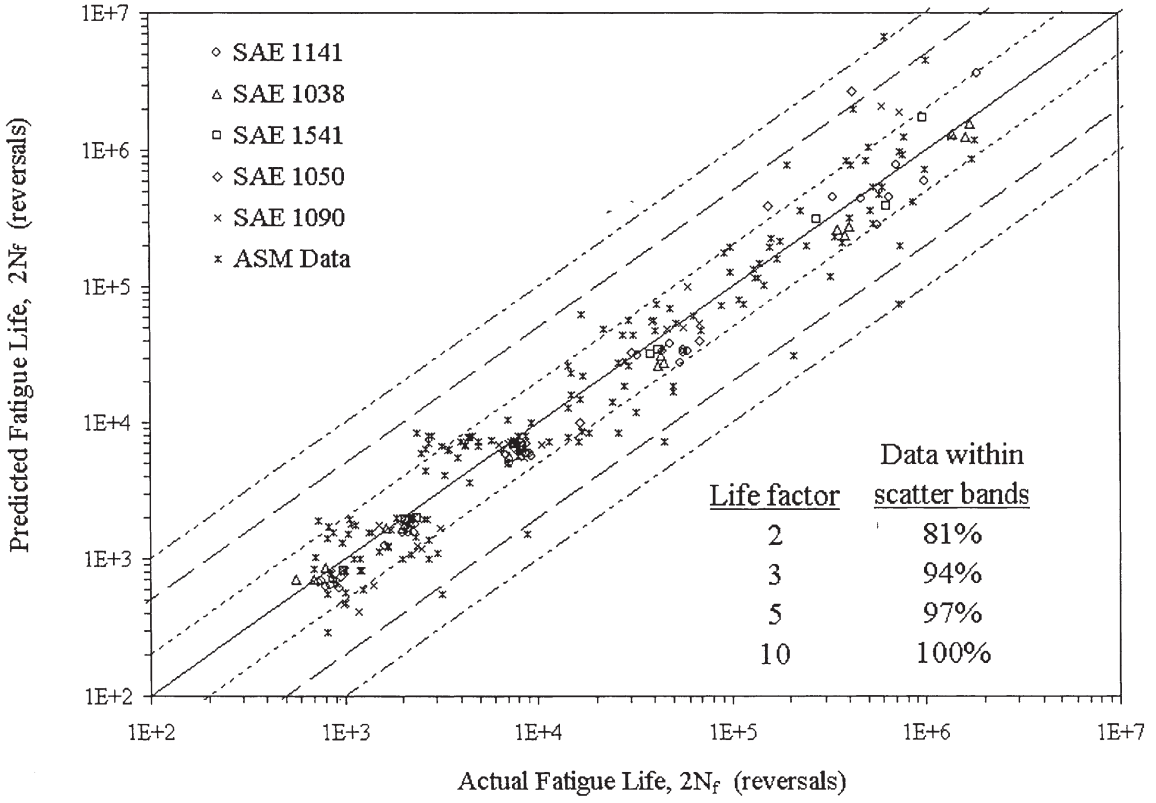

Fig. 18. Prediction of fatigue life by the proposed method.

1. A strong correlation exists between hardness and ultimate tensile strength of steels. A second order polynomial is found to provide a better fit to the data, as compared with a commonly used linear fit.
2. Correlations between the fatigue limit and ultimate tensile strength were weak, with significant scatter. A commonly used estimate of fatigue limit as half of the ultimate tensile strength was found to be nonconservative for the great majority of steels. Correlation of fatigue limit with hardness was found to be better than with the ultimate tensile strength.
3. A relatively strong correlation was found between the transition fatigue life and hardness. A relationship proposed in the literature provided good predictions of the transition fatigue life based on hardness for most of the data.
4. No strong correlation was found between the fatigue strength coefficient and the true fracture strength. Better correlations of the fatigue strength coefficient were found with the ultimate tensile strength and hardness.
5. No correlations were found between the fatigue ductility coefficient and the true fracture ductility. Using the true fracture ductility to approximate the fatigue ductility coefficient can result in significant error.
6. Three relationships estimating the strain–life curve from monotonic tensile properties were evaluated. These three estimates had been found to provide good approximations of the strain–life curve in another study and consist of the Modified Universal Slopes Method, the Uniform Material Method, and the Modified Four-Point Correlation Method. Similar and satisfactory predictions from these three methods were also obtained for the data in this study.
7. A simple method is proposed for estimation of the strain–life curve. This method only requires hardness and modulus of elasticity as inputs, both of which are either commonly available or easily measurable. Prediction capability of the proposed method was evaluated for steels with hardness in the range between 150 and 700 HB. The proposed method is shown to provide good approximations of the strain–life curve and result in somewhat better predictions of the strain amplitudes or fatigue lives over the entire fatigue life regime, compared to several methods proposed in the literature.

Acknowledgements

We would like to thank the American Iron and Steel Institute (AISI) for financial support of this project. We also acknowledge Dr T. Topper and his research assistants from the University of Waterloo for their collaborative efforts in obtaining the material properties for SAE 1541, SAE 1050, and SAE 1090 steels used in this study.

References

[1] Bauccio M, editor. ASM Metals Reference Book, 3rd ed. Materials Park, OH: ASM International, 1993.
[2] ASTM Standard E1012-93a, Standard Practice for Verification of Specimen Alignment Under Tensile Loading. Annual Book of ASTM Standards, vol. 03.01. American Society for Testing and Materials, West Conshohocken, PA. 1997:699–706.
[3] ASTM Standard E8-96a, Standard Test Methods for Tension Testing of Metallic Materials. Annual Book of ASTM Standards, vol. 03.01. American Society for Testing and Materials, West Conshohocken, PA. 1997:56–76.
[4] ASTM Standard E606-92, Standard Practice for Strain-Controlled Fatigue Testing. Annual Book of ASTM Standards, vol. 03.01. American Society for Testing and Materials, West Conshohocken, PA. 1997:523–537.
[5] Bridgman PW. Stress distribution at the neck of tension specimen. Transactions of the American Society for Metals 1944;32:553–72.
[6] ASTM Standard E646-93, Standard Test Method for Tensile Strain-Hardening Exponents (*n*-values) of Metallic Sheet Materials. Annual Book of ASTM Standards, vol. 03.01. American Society for Testing and Materials, West Conshohocken, PA. 1997: 550–556.
[7] Roessle ML, Fatemi A, Khosrovaneh AK. Variation in Cyclic Deformation and Strain-Controlled Fatigue Properties using Different Curve Fitting and Measurement Techniques. SAE Paper 1999-01-0364. 1999:1-8.
[8] Mitchell MR, Socie DF, Caulfield EM. Fundamentals of Modern Fatigue Analysis. Fracture Control Program Report No. 26, University of Illinois, USA. 1977:385-410.
[9] Stephens RI, Fatemi A, Stephens RR, Fuchs HO. Metal Fatigue in Engineering. 2nd ed. Wiley Interscience, 2000.
[10] Landgraf RW. The Resistance of Metals to Cyclic Deformation. Achievement of High Fatigue Resistance in Metals and Alloys—ASTM STP 467. American Society for Testing and Materials, Philadelphia, PA, 1970:3-36.
[11] Morrow JD. Cyclic Plastic Strain Energy and Fatigue of Metals. Internal Friction, Damping, and Cyclic Plasticity—ASTM STP 378. American Society for Testing and Materials, Philadelphia, PA, 1964:45-87.
[12] Park J, Song J. Detailed evaluation of methods for estimation of fatigue properties. International Journal of Fatigue 1995;17(5):365–73.
[13] Manson SS. Fatigue: a Complex Subject—Some Simple Approximations. Experimental Mechanics—Journal of the Society for Experimental Stress Analysis 1965;5(7):193–226.
[14] Muralidharan U, Manson SS. Modified universal slopes equation for estimation of fatigue characteristics. Journal of Engineering Materials and Technology—Transactions of the American Society of Mechanical Engineers 1988;110:55–8.
[15] Bäumel A Jr., Seeger T. Materials Data for Cyclic Loading, Supplement I. Amsterdam: Elsevier Science Publishers, 1990.
[16] Ong JH. An improved technique for the prediction of axial fatigue life from tensile data. International Journal of Fatigue 1993;15(3):213–9.
[17] Ong JH. An evaluation of existing methods for the prediction of axial fatigue life from tensile data. International Journal of Fatigue 1993;15(1):13–9.